PREPRINT UCRL-80460

Lawrence Livermore Laboratory

PRESUPERNOVA EVOLUTION OF MASSIVE STARS

Thomas A. Weaver and George B. Zimmerman
University of California Lawrence Livermore Laboratory

and

S. E. Woosley
University of California, Santa Cruz
and Lawrence Livermore Laboratory

December 15, 1977

This paper was prepared for submission to The Astrophysical Journal.

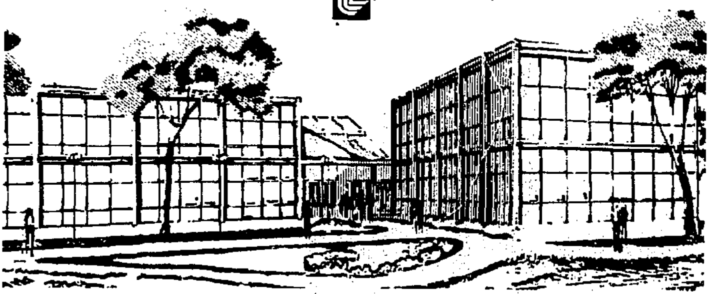

PRESUPERNOVA EVOLUTION OF MASSIVE STARS

Thomas A. Weaver and George B. Zimmerman
University of California Lawrence Livermore Laboratory*

and

S. E. Woosley
University of California, Santa Cruz†
and Lawrence Livermore Laboratory

ABSTRACT

Population I stars of 15 $M_{\odot}$ and 25 $M_{\odot}$ have been evolved from the zero-age *main sequence* through iron core collapse utilizing a numerical model that incorporates both implicit hydrodynamics and a detailed treatment of nuclear reactions. The stars end their presupernova evolution as red supergiants with photospheric radii of 3.9×10^{13} cm and 6.7×10^{13} cm, respectively, and density structures similar to those invoked to explain Type II supernova light curves on a strictly hydrodynamic basis. Both stars are found to form substantially neutronized "iron" cores of 1.56 $M_{\odot}$ and 1.61 $M_{\odot}$, and central electron abundances of 0.427 and 0.439 moles/g, respectively, during hydrostatic silicon burning. Just prior to collapse, the abundances of the elements in the 25 $M_{\odot}$ star (excluding the neutronized iron core) have ratios strikingly close to their solar system values over the mass range from oxygen to calcium, while the 15 $M_{\odot}$ star is characterized by large enhancements of Ne, Mg, and Si. It is pointed out on *nucleosynthetic* grounds that the mass of the neutronized core must represent a lower limit to the mass of the neutron star or black hole remnant that stars in this mass range can normally produce.

* Work performed under the auspices of U.S. DoE under Contract No. W-7405-Eng-48.
† Work performed in part under NSF Contract No. AST 76-10933.

I. INTRODUCTION

In this paper we report the first detailed calculations of the evolution of complete 15 and 25 $M_\odot$ population I stars from the zero-age main sequence through iron core collapse. Unlike most previous studies of advanced stellar evolution (especially post-neon burning), we have calculated the structure of entire stars instead of just helium, carbon, or oxygen "cores" (c.f. Arnett 1972 abc, 1973a, 1974ab, 1977; Barkat 1971; Ikeuchi, et al. 1971, 1972; Sugimoto 1970, 1971; and Rakavy, Shaviv, and Zinamon 1967), and have given very careful consideration to the quite complex nuclear processes that characterize the final evolutionary stages.

This work represents the first step of a comprehensive program to calculate both the hydrostatic and explosive phases of the evolution of massive stars (10-50 $M_\odot$) and to predict in detail the isotopic abundances that result. The long-term aim is to achieve a self-consistent and, as far as possible, parameter-free synthesis between stellar evolution and the various nuclear processes believed responsible for the production of the chemical elements.

The primary purpose of this paper is to present the configurations of the 15 and 25 $M_\odot$ stars at the beginning of core collapse and to discuss their implications for nucleosynthesis and the supernova explosions thought to follow. In a subsequent series of papers, we will discuss in greater detail both our dynamic stellar model and the various stages of hydrostatic nuclear burning, including extensive comparison with previous work and additional results for 10, 20, 35, and 50 $M_\odot$ stars

II. HYDRODYNAMIC STELLAR MODEL

In order to study both the static and dynamic phases of stellar evolution, an implicit hydrodynamics computer code (KEPLER) has been developed which integrates the equations of motion and heat transfer assuming spherical symmetry and consequently the absence of rotation and magnetic fields. These equations, when expressed in Lagrangian (co-moving) coordinates, and using the mass interior to a given radius, m, as the independent variable, take the form:

$$\frac{dv}{dt} = -4\pi r^2 \frac{\partial P}{\partial m} - \frac{Gm}{r^2} + \frac{4\pi}{r} \frac{\partial Q}{\partial m} \tag{1}$$

$$\frac{d\varepsilon}{dt} = -4\pi P \frac{\partial}{\partial m}(vr^2) + 4\pi Q \frac{\partial}{\partial m}\left(\frac{v}{r}\right) - \frac{\partial L}{\partial m} + \dot{S} \tag{2}$$

where r is the radius; $v = dr/dt$, the velocity; P, the pressure; ε, the internal energy per unit mass; Q, the artificial viscous stress required to treat shock waves (c.f. Richtmyer 1957); L, the rate of energy flow (luminosity) through a shell of radius $r(m)$; $\dot{S}$, the local energy generation rate per unit mass; and G, the gravitational constant.

The implicit solution of these equations requires that one express these various quantities in terms of the dependent variables ρ (density), T (temperature), and L, linearize the resulting equations, and solve them in forward-time-differenced form for the changes in ρ, T, and L during time interval Δt. In general, this procedure involves calculating the partial derivatives of P, ε, $\dot{S}$, and L with respect to density and temperature (with material composition held constant), and iterating until the full non-linear equations are satisfied. Changes in composition due to convective mixing and nuclear burning are then calculated explicitly using the converged values of ρ and T. This procedure is analogous to the quasistatic relaxation method employed by Henyey, et al. (1959, 1964) and yields the correct hydrostatic and thermal equilibrium solutions when the time steps taken are large compared with the characteristic equilibration times.

The equation of state employed to relate pressure and energy to the temperature and density allows for electrons and positions of arbitrary relativity and degeneracy (in the perfect gas approximation), using Divine's (1966) approximation to evaluate the necessary relativistic Fermi integrals. This approximation becomes exact in the limits of extreme (non)degeneracy and (non)relativity and introduces an error of at most 0.3% in the intermediate regime. The ions are treated as a nonrelativistic perfect gas with allowance made for nuclear degeneracy, while the radiation field is assumed to be in local thermodynamic equilibrium. Ionization and pressure ionization are included using a simplified "average atom" model which suffices to give a good approximation to the electron pressure.

The radiative and conductive opacities are calculated using the analytic prescription of Iben (1975) based on the results of Christy (1966), Cox and Stewart (1970ab), Canuto (1970), and Hubbard and Lampe (1969), except that a new fit to the Compton scattering opacity was made to include the effects of degeneracy and relativity.

An innovative time-dependent method of treating convection and semiconvection has been employed which uses standard mixing length theory (c.f. Clayton, 1968) to calculate the heat flux and average velocity (v_c) of a convective element, using a mixing length (ℓ) equal to the pressure scale height. Mixing of ion species abundances (Y_i) in a convective region is performed by solving the time dependent diffusion equation given by:

$$\frac{dY_i}{dt} = \frac{\partial}{\partial m}\left\{(4\pi r^2)^2 \rho^2 D \frac{\partial Y_i}{\partial m}\right\} \quad (3)$$

where the diffusion coefficient, D, is given by $D = D_c \equiv v_c \ell/3$ when the material is convective by the Ledoux (density gradient) criterion, by $D = D_s \equiv q_r D_c D_R/(D_c+D_R)$ when the material would be convective by the Schwarschild (temperature gradient) criterion but not by the Ledoux criterion, and is zero otherwise. Here D_R is the radiation diffusion constant and q_r is an adjustable parameter which has been taken as 0.1. Non-convective spatial zones immediately adjacent to convective regions are also slowly mixed on the order of a radiation diffusion time scale to approximately allow for the effects of convective overshoot, and in particular, to allow for cases where such overshoot causes convective regions to grow. Convective heat transport is assumed to occur only when the material is convective by the Ledoux criterion.

This prescription reflects the physical fact that a medium is only dynamically unstable to convection if the Ledoux criterion is satisfied (i.e., when the buoyancy force acting on a mass element overbalances gravity), while a region that would be "convective" by the Schwarzschild but not the Ledoux criterion (due to composition gradients) can at most be characterized by a secular instability that grows into a dynamic instability over a time longer than the thermal (and thus radiative) diffusion time (c.f. Speigel 1969). Indeed, only fully established (Ledoux) convection can be expected to carry a significant amount of convective heat flow. This prescription also allows implicitly for what is usually termed "semi-convection" by causing the composition gradients to be naturally and dynamically adjusted toward a condition of convective neutrality in ("semi-convective") regions where partial material mixing is sufficient to quench convection due to changes in the opacity or molecular weight gradients.

Nuclear reactions are treated using two distinct networks. The first is a flexible 19-element (82-reaction) network capable of efficiently generating accurate nuclear energy generation rates for nuclear processes ranging from hydrogen burning to the beginning of hydrostatic silicon burning. This network includes: ^{1}H, ^{3}He, ^{4}He, ^{12}C, ^{14}N, ^{16}O, ^{20}Ne, ^{24}Mg, ^{28}Si, ^{32}S, ^{36}Ar, ^{40}Ca, ^{44}Ti, ^{48}Cr, ^{52}Fe, ^{54}Fe, ^{56}Ni, protons (from photodisintegration), and neutrons. In addition, flows proceeding through the elements ^{27}Al, ^{31}P, ^{35}Cl, ^{39}K, ^{43}Sc, ^{47}V, ^{51}Mn, ^{55}Co, ^{53}Fe, and ^{2}H are included implicitly, by assuming that their abundances are in steady state with neighboring nuclei. Except for ^{2}H, these reactions involve (α,p), (p,γ) links between adjacent α-particle nuclei, and are included in the network as augmented (α,γ) links. Thermal neutrino losses are calculated using the fit given by Beaudet, Petrosian, and Salpeter (1967; henceforth BPS) while the general nuclear Coulomb screening prescription of Graboske, DeWitt, Grossman, and Cooper (1973) (which is accurate in the weak and intermediate screening cases of present interest) was used. Most of the strong and electromagnetic rates employed are due to Fowler, Caughlan, and Zimmerman (1975) and Woosley, et al.(1975).

In order to accurately treat the complex neutronization process that occurs during hydrostatic silicon burning, a 121-isotope network was employed under conditions where the nuclear abundances could be reasonably represented by a quasi-equilibrium (QSE) distribution (see Bodansky, Clayton, and Fowler, 1968). The rate of change of the electron abundance (Y_e), and thus the degree of neutronization and associated neutrino loss rate, is calculated from Mazarek's (1973) electron capture rates where available (81 cases), and otherwise from those of Hansen (1966), if possible (21 cases). In addition, electron decay rates for 63 isotopes and positron decay rates for 83 isotopes are taken into account using Hansen's (1966) rates, and accurate fits are used for the electron capture rate on free protons and the positron capture rate on free neutrons (Tubbs 1977). The QSE network isotopes included are: n, $^{1-3}$H, $^{3-5}$He, ^{5}Li, ^{12}C, ^{16}O, ^{20}Ne, ^{23}Na, $^{24-26}$Mg, $^{27-28}$Al, $^{28-30}$Si, $^{31-33}$P, $^{32-34}$S, $^{35-37}$Cl, $^{36-40}$Ar, $^{39-43}$K, $^{40-44,46,48}$Ca, $^{43-49}$Sc, $^{44-52}$Ti, $^{47-54}$V, $^{48-56}$Cr, $^{51-58}$Mn, $^{52-62}$Fe, $^{54-64}$Co, $^{56-66}$Ni, ^{59}Cu and ^{60}Zn. The fits of Holmes, et al. (1976) to the temperature dependent nuclear partition functions, and the nuclear binding energies given by Wapstra and Bos (1976) are incorporated in the QSE calculation; and a natural transition to full nuclear statistical equilibrium is provided. This QSE network should be adequate to yield accurate abundances for $0.5 \geq Y_e \geq 0.43$, $\rho \leq 10^{12}$ g/cc, and $T \leq 10^{10}$°K.

III. RESULTS AND DISCUSSION

The initial composition (by mass) of the 15 and 25 $M_\odot$ stars was taken to be 70% H, 28% He, and 2% heavy elements in proportions given by Cox and Stewart's (1970ab) Population I element mix. The initial configuration was a "cloud" with a mean density of 0.5 g/cc and a temperature profile adjusted to give hydrostatic equilibrium. The results are insensitive to the initial thermodynamic configuration, and the stars quickly relax to their well-known zero-age main sequence structures.

Table I summarizes the subsequent evolution of these stars through the various stages of "hydrostatic" nuclear burning. In general, our results through He burning agree quite closely with those of Lamb, Iben, and Howard (1977), but do not agree well with those of Endal (1975ab). A direct comparison with Arnett's (1972abc, 1973a, 1974ab, 1977) helium core models is difficult to make, but the 15 $M_\odot$ star is qualitatively similar to Arnett's 4 $M_\odot$ He core, while the 25 $M_\odot$ star roughly corresponds to his 8 $M_\odot$ He core.

Figures 1, 2, and 3 show the composition and thermodynamic structure of the 15 and 25 $M_\odot$ stars at a point early in iron core collapse when peak collapse velocities have reached $\approx$ 1000 km/sec. The core collapse is a natural result of the preceding evolution and is in no way artificially induced. The salient features of those presupernova models are discussed in the following sections.

a) Density Structure

The general structure of both presupernova stars is that of a red supergiant with a high density mantle $\sim 3\times10^{10}$ cm in radius surrounded by a very low density envelope with a nearly constant $\rho \approx 10^{-8}$ g/cc and $T \approx 10^{5}$°K which extends out to the photospheric radius of 3.9×10^{13} cm (15 $M_\odot$) or 6.7×10^{13} cm (25 $M_\odot$). This is quite similar to the density structures which Falk and Arnett (1973, 1977) and Chevalier (1976) have invoked to explain Type II supernova light curves on a purely hydrodynamic basis. The structure of the envelopes of these stars has been essentially frozen since the beginning of carbon burning, when neutrino losses replaced photospheric emission as the stars' dominant energy sink and dramatically increased the speed of the cores' evolution.

b) Shell Structure

It is evident that both stars have evolved into an "onionskin" structure with distinct H, He, C, Ne, O, and Si burning shells. These shells are typically convective, and are separated by sufficiently sharp density (entropy) gradients to prevent convective material mixing between them.

c) Hydrostatic Neutronization

Hydrostatic silicon burning occurs over a sufficiently long time scale that the iron peak elements that result are substantially neutronized by electron capture during the burning itself. The resulting "iron" cores have masses of 1.56 $M_\odot$ and 1.61 $M_\odot$, and central electron abundances of 0.427 and 0.439 moles/g, respectively, for the 15 and 25 $M_\odot$ stars. Note that this is already below the range of Y_e for which Epstein and Arnett (1975) studied neutronization during core collapse. The composition is dominated by very neutron-rich species such as ^{48}Ca, ^{66}Ni, ^{54}Cr, and ^{50}Ti near the center and gradually shifts through progressively less neutron-rich species, dominated successively by ^{58}Fe, ^{56}Fe, and ^{54}Fe, as one proceeds outward.

The region around $Y_e = 0.46$ where ^{56}Fe is the dominant iron peak constituent (as it is observed to be in the solar system) covers at most a few tenths of a solar mass, while non-neutronized iron ($Y_e = 0.50$, i.e. ^{56}Ni or $^{54}Fe + 2p$), which beta decays naturally to the observed iron abundances, is present only in the narrow flashing region of the 25 $M_\odot$ star's silicon shell located at $m = 1.65\ M_\odot$. The discontinuities in composition and Y_e at an interior mass of approximately 1 $M_\odot$ are a fossil remnant of the outermost extent of the central convective region during core silicon burning, and similarly the abrupt fall in Y_e at the edge of the iron core represents the outermost extent of the convective region associated with shell silicon burning. It is important to note that this convective mixing has allowed the iron cores to grow substantially beyond the Chandrasekhar mass ($\gtrsim$ 1.2-1.3 $M_\odot$ for the current Y_e profiles) before collapse. The general character of these results appears relatively insensitive to the choice of electron-capture rates. Specifically, a test case in which Hansen's (1966) rates were used instead of Mazarek's (1973) rates to evolve the 25 $M_\odot$ star still resulted in $Y_e \lesssim 0.44$ in the core, a similar convective structure, and silicon shell burning to ^{54}Fe. Another interesting feature of concurrent silicon burning and neutronization is that a substantial amount of energy (typically 2-5 times the normal convective energy flux) is transported outward by convective mixing of short-lived radioactive species (particularly ^{56}Ni) which provide thermal heat input upon decay.

d) Collapse Energetics

It is apparent from Figures 1 and 2 that photodisintegration of the iron-peak elements to alpha particles provides the dominant source of core energy loss during the early stages of collapse. Neutrino losses due to neutronization and thermal plasma (BPS) processes are about a factor of 30 and 1000, respectively, less important, and the Y_e profile has not yet changed significantly from its hydrostatic value.

e) Nucleosynthesis

Figure 6 shows the enhancement of the presupernova elemental abundances relative to Cameron's (1973) solar system abundances. The contributions of the neutronized iron cores, which are presumed to collapse, have been omitted. It is apparent that for the 25 $M_\odot$ star the elements between oxygen and calcium are uniformly enhanced by a factor of about 35, while carbon, nitrogen, and the iron peak elements are relatively underproduced in both stars. The 15 $M_\odot$ star is predominantly enhanced in Ne, Mg, and Si (by a factor of ~ 30), but curiously produces C, N, and O in their relative solar system ratios, although with an overall enhancement of only 5.5.

In order to make any compelling connections between these stellar abundances and observed solar system abundances, it is necessary to consider the effects of explosive nuclear burning, the position of the "mass cut" between ingoing and outgoing material in the supernova explosion, and the relative population of these and other stars in the galactic disk. While these issues will be addressed in detail in future calculations, the following preliminary observations can be made:

i) Explosive Nucleosynthesis. While the abundances of elements between oxygen and calcium in the 25 $M_\odot$ star cluster around an enhancement factor of 35 within the probable factor-of-two errors in the solar abundance determinations, it is evident that there is a systematic trend for the lighter elements to have larger enhancements, and that except for neon (whose solar abundance is particularly uncertain), the ratios between adjacent mass elements agree with their solar ratios to within about 20%. If not balanced out by contributions from different mass stars, this trend may indicate the magnitude of the role explosive nucleosynthesis will have to play in order to "level" the post supernova abundance distribution into precise agreement with solar values. It is well worth noting in this regard that while neither star has yet made much non-neutronized iron (i.e., iron of acceptable solar isotopic composition) at the early collapse stage shown in Figures 1-2, the 25 $M_\odot$ star contains an actively burning silicon shell that produces about 0.15 $M_\odot$ and ^{56}Ni and $^{54}Fe + 2p$ as the core collapse continues. This "implosive nucleosynthesis" increases the relative iron abundance to the point indicated in Figure 6 by the circled star, and almost certainly persists to become explosive silicon burning during the core expansion that must follow if this material is to be ejected into the interstellar medium. Such behavior suggests strongly that mass 56 is synthesized as ^{56}Ni, not ^{56}Fe, with resultant implications for γ-ray astronomy (Clayton, Colgate, and Fishman, 1969).

For reasonably strong outgoing shock waves ($E_s \gtrsim 10^{51}$ ergs), some explosive oxygen and perhaps neon processing also seems likely on the basis of preliminary calculations. The nucleosynthesis that occurs in the extensive regions rich in Ne, O, and Mg with a few per cent C will be particularly interesting (the moreso for having been almost completely unexplored to date). A collaborative effort is currently under way to use the presupernova models given here as the initial input for Wilson's (1971, 1974, 1977ab) detailed supernova core computer code. After the core's evolution has been followed through collapse, bounce, and (hopefully) outward-going shock wave formation, the core conditions will be "linked" back into KEPLER to calculate the ensuing explosive nucleosynthesis. This should represent an enormous improvement over past calculations that employed simple parameterized representations of the density and temperature history (c.f. Woosley, Arnett, and Clayton 1973 and Arnett 1973b).

ii) Supernova Remnant Mass. The neutronized iron cores present in both the 15 and 25 $M_\odot$ star contain such a large quantity of ^{54}Fe and rare highly neutronized iron peak species that, in order to prevent massive overproduction of these isotopes, virtually the entire core must normally collapse to form a neutron star or black hole remnant. Specifically, in order for the enhancement factor of ^{54}Fe not to exceed 35, less than 0.03 $M_\odot$ of the material just inside the core boundary can be ejected on the average. These nucleosynthetic considerations thus set a fairly high lower limit on the mean mass of the supernova remnants formed by stars in this mass range, and, indeed, the similarity of the 15 and 25 $M_\odot$ cores suggests such a lower limit may apply over a much wider mass range.

iii) Relative Stellar Contributions to Nucleosynthesis. When the neutronized iron cores are omitted, one sees from Figures 1 and 2, that the 25 $M_\odot$ star can potentially eject 6.2 $M_\odot$ of heavy ($Z > 2$) elements into the interstellar medium, whereas the 15 $M_\odot$ star can eject at most 1.1 $M_\odot$. Using the Salpeter (1955) initial stellar mass function, nne finds that 15 $M_\odot$ stars are "born" roughly a factor of $(15/25)^{-1.35} = 2$ more frequently than

25 $M_\odot$ stars. It thus appears that 25 $M_\odot$ stars potentially account for about a factor of 3 more heavy element production than 15 $M_\odot$ stars, which is encouraging given their more closely solar abundance ratios.

Carbon and nitrogen are underproduced in both stars studied here, and one may need to invoke production of these species in lower mass stars where they might be injected into the interstellar medium by convective mixing and mass loss as suggested by the planetary nebula observations of Shields (1978). Other possibilities include invoking a mass cut just inside the helium-burning shell for some restricted mass range or type of massive stars, or ejecting unprocessed carbon in lower mass supernovae ($M \lesssim 8\ M_\odot$) that ignite carbon burning degenerately (Arnett 1969; Chechetkin, et al. 1977).

ACKNOWLEDGEMENTS

We are grateful to Lowell Wood and Edward Teller for their encouragement, support, and useful suggestions, to George Fuller and John Zyskind for help in formulating parts of the equation of state and nuclear reaction prescriptions, to Ted Mazarek for supplying his weak rate data in convenient form, and to W. A. Fowler, J. R. Wilson, D. N. Schramm, D. L. Tubbs, S. A. Lamb, and W. M. Howard for useful discussions. The hospitality and stimulating atmosphere of the 1976 Aspen Center of Physics Nucleosynthesis Workshop and the 1977 UC Santa Cruz Supernova Workshop are also gratefully acknowledged.

REFERENCES

Arnett, W. D. 1969, Astrophys. Space Sci., 5, 180.

__________. 1972a, Ap.J., 176, 681.

__________. 1972b, Ap.J., 176, 699.

__________. 1972c, Ap.J., 173, 393.

__________. 1973a, Ap.J., 179, 249.

__________. 1973b, Ann. Rev. Astr. and Ap., 11, 73.

__________. 1974a, Ap.J., 193, 169

__________. 1974b, Ap.J., 194, 373.

__________. 1977, Ap.J. Suppl., in press.

Barkat, Z. 1971, Ap. J., 163, 433.

Beaudet, G., Petrosian, V., and Salpeter, E. E. 1967, Ap.J., 150, 979 (BPS).

Bodansky, D., Clayton, D. D., and Fowler, W. A. 1968, Ap.J. Suppl., 16, 299.

Cameron, A. G. W. 1973, Space Sci. Rev., 15, 121.

Canuto, V. 1970, Ap. J., 159, 641.

Chechetkin, V. M., Imshennik, V.S., Ivanova, L. N., and Nadyozhin, D. K. 1977, Supernovae, D. N. Schramm (ed.) (Dordrecht-Holland: Reidel), p. 159.

Chevalier, R. 1976, Ap. J., 207, 872.

Christy, R. F. 1966, Ap. J., 144, 108.

Clayton, D. D. 1968, Principles of Stellar Evolution and Nucleosynthesis (New York: McGraw-Hill).

Clayton, D. D., Colgate, S. A., and Fishman, G. J. 1969, Ap. J., 155, 75.

Cox, A. N. and Stewart, J. N. 1970a, Ap. J. Suppl., 19, 243.

__________. 1970b, Ap. J. Suppl., 19, 261.

Divine, N. 1966, Ap. J., 142, 1652.

Endal, A. S. 1975a, Ap. J., 195, 187.

__________. 1975b, ibid. 197, 405.

Epstein, R. I. and Arnett, W. D. 1975, Ap. J., 201, 202.

Falk, S. W. and Arnett, W. D. 1973, Ap. J. (Letters), 180, L65.

________________________. 1977, Ap. J. Suppl., 33, 515.

Fowler, W. A., Caughlan, G. R., and Zimmerman, B. A. 1975, Ann. Rev. Astr. and Ap., 13, 69.

Graboske, H. C., DeWitt, H. E., Grossman, A. S., and Cooper, M. S. 1973, Ap. J., 181, 457.

Hansen, C. J. 1966, Ph.D. Thesis, Yale University (unpublished).

Henyey, L. G., Forbes, J. E., and Gould, N. L. 1964, Ap. J., 139, 306.

Henyey, L. G., Wilets, L., Böhm, K. H., LeLevier, R., and Levee, R. D. 1959, Ap. J., 129, 628.

Holmes, J. A., Woosley, S. E., Fowler, W. A., and Zimmerman, B. A. 1976, Atomic Data and Nuclear Data Tables, 18, 305.

Hubbard, W. B. and Lampe, M. 1969, Ap. J. Suppl., 18, 279.

Iben, I., Jr. 1975, Ap. J., 196, 525.

Ikeuchi, S., Nakazawa, K., Murai, T., Hoshi, R., and Hayashi, C. 1971, Prog. Theor. Phys., 46, 1713.

________________________. 1972, ibid., 48, 1870.

Lamb, S. A., Iben, I., Jr., and Howard, W. M. 1976, Ap. J., 207, 209.

Mazurek, T. 1973, Ph.D. Thesis, Yeshiva University (unpublished).

Rakavy, G., Shaviv, G., and Zinamon, Z. 1967, Ap. J., 150, 131.

Richtmyer, R. D. 1957, Difference Methods for Initial Value Problems (New York: Interscience).

Salpeter, E. E. 1955, Ap. J., 121, 161.

Shields, G. A. 1978, Ap. J., Jan. 15, in press.

Spiegel, E. A. 1969, CASP, 1, 57.

Sugimoto, D. 1970, Progr. Theoret. Phys., 44, 599.

__________. 1971, ibid., 45, 461.

Tubbs, D. L. 1977, private communication.

Wapstra, A. H. and Bos, K. 1976, Atomic and Nucl. Data Tables, 17, 474.

Wilson, J. R. 1971, Ap. J., 163, 209.

__________. 1974, Phys. Rev. Lett., 32, 849.

REFERENCES (Continued)

Wilson, J. R. 1977a, Varrena Lectures, to be published.

__________. 1977b, preprint.

Woosley, S. E., Fowler, W. A., Holmes, J. A., and Zimmerman, B. A. 1975, OAP-422 and Atomic Data and Nuclear Data Tables, to be published.

Woosley, S. E., Arnett, W. D., and Clayton, D. D. 1973, Ap. J. Suppl., 26, 231.

TABLE I

Major Nuclear Burning Stages for 15 and 25 $M_\odot$ Pop I Stars*

Burning Stage	Central Temperature (K)	Central Density (g cm^{-3})	Neutrino Luminosity† (erg s^{-1})	Optical Luminosity (erg s^{-1})	Effective Temperature (K)	Photospheric Radius (cm)	Time Scale (s)
Hydrogen	3.4 (7) 3.7 (7)	5.9 (0) 3.8 (0)	---- ----	8.1 (37) 3.1 (38)	3.26 (4) 3.98 (4)	3.2 (11) 4.2 (11)	3.9 (14) 2.3 (14)
Helium	1.6 (8) 1.8 (8)	1.3 (3) 6.[illegible] (2)	3.9 (33) 7.3 (34)	2.3 (38) 9.5 (38)	1.59 (4) 1.58 (4)	2.2 (12) 4.7 (12)	4.2 (13) 2.1 (13)
Carbon	6.2 (8) 7.2 (8)	1.7 (5) 6.4 (5)	3.4 (38) 1.0 (40)	3.3 (38) 1.2 (39)	4.26 (3) 4.36 (3)	3.7 (13) 6.7 (13)	2.0 (11) 5.2 (9)
Neon	1.3 (9) 1.4 (9)	1.6 (7) 3.7 (6)	6.7 (41) 7.8 (42)	3.7 (38) 1.2 (39)	4.28 (3) 4.36 (3)	3.9 (13) 6.7 (13)	2.2 (8) 3.9 (7)
Oxygen	1.9 (9) 1.8 (9)	9.7 (6) 1.3 (7)	7.9 (42) 2.3 (43)	3.7 (38) 1.2 (39)	4.28 (3) 4.36 (3)	3.9 (13) 6.7 (13)	5.5 (7) 1.6 (7)
Silicon	3.1 (9) 3.4 (9)	2.3 (8) 1.1 (8)	3.4 (44) 3.8 (45)	3.7 (38) 1.2 (39)	4.28 (3) 4.36 (3)	3.9 (13) 6.7 (13)	5.2 (5) 1.2 (5)
Collapse	8.3 (9) 8.3 (9)	6.0 (9) 3.5 (9)	6.8 (48) 8.1 (48)	3.7 (38) 1.2 (39)	4.28 (3) 4.36 (3)	3.9 (13) 6.7 (13)	3.0 (-1) 3.5 (-1)

*All physical parameters refer to conditions just after the core ignition of each fuel, except the time scale which is the period between successive ignitions. The value for the 15 $M_\odot$ star is listed first in each case.

†Excluding neutrino losses during hydrogen burning.

FIGURE CAPTIONS

Figure 1. The composition (a) and thermodynamic structure (b) of the 15 $M_{\odot}$ star at the beginning of core collapse. In the inner 1.56 $M_{\odot}$, where the QSE network was employed, the curve labeled ^{56}Ni includes all iron peak species with $A \approx 2Z$, ^{54}Fe, all those with $A \approx 2(Z+1)$, and "Fe", all other QSE network elements with $Z \geq 22$ (e.g. ^{56}Fe, ^{58}Fe, etc.). Note that the density and temperature profiles are plotted such that the curves will maintain constant separation for the case $\rho \propto T^3$. Here $-\dot{S}_T$ is the total local energy loss rate due to both neutrino emission and nuclear photodisintegration, $\dot{S}_\nu$ is the total neutrino energy loss rate, and $\dot{S}_{\nu P}$ is the neutrino energy loss rate due to the thermal plasma processes given by BPS. The nuclear energy generation rate profiles for the various nuclear burning shells are labeled $\dot{S}_N$ and the principal nuclear fuel is indicated. All energy generation and loss rates share the common scale denoted by S. Active convective regions are indicated by striped bars, while semi-conductive and convectively neutral regions are shown as outlined bars. In this figure, R, T_{eff}, and L denote the photospheric radius, effective temperature, and optical luminosity, respectively.

Figure 2. The composition (a) and thermodynamic structure (b) of the 25 $M_{\odot}$ star at the beginning of core collapse. All notation is the same as that of Figure 1, except that the QSE network was employed in the inner 1.61 $M_{\odot}$ of the star.

Figure 3. Electron abundance (Y_e) and collapse velocity (v) profiles at the beginning of core collapse.

Figure 4. Elemental enhancement factors relative to hydrogen at the beginning of core collapse, assuming all radioactive species have decayed. The enhancement factor is defined as: $(M_Z - \Delta M_{ZI})/M_H\, R_{Z\odot}$, where M_Z is the total mass of element Z in the star (excluding the neutronized core), M_H is the total mass of hydrogen, $R_{Z\odot}$ is the ratio of the solar mass fraction of element Z to that of hydrogen as given by Cameron (1973), and $\Delta M_{ZI} = M_{ZI} - M_{HI}R_{Z\odot}$ where M_{HI} is the initial mass of hydrogen in the star and M_{ZI}, the initial mass of element Z. The ΔM_{ZI} term is only important for small enhancements and corrects for enhancements resulting from differences between the initial stellar abundances and Cameron's solar abundances. Note that enhancements arise due to both the production of the element involved and the depletion of hydrogen relative to its initial value (by factors of 0.65 and 0.51, respectively, for the 15 and 25 $M_\odot$ stars). The symbol <Fe> denotes iron peak elements, and the circled star shows the results of implosive silicon burning in the 25 $M_\odot$ star.

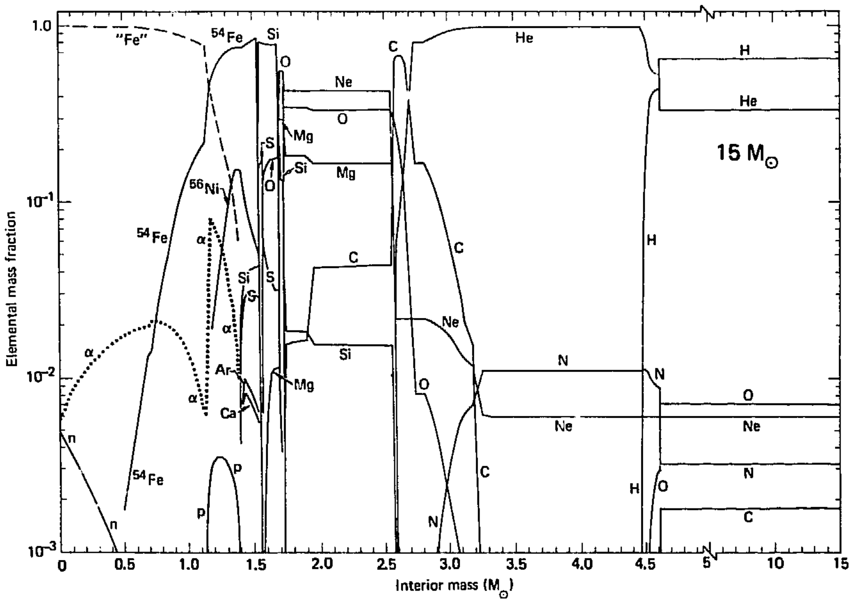

Elemental mass fraction
Interior mass (M⊙)
15 M⊙
"Fe"
54Fe
56Ni
α
n
p
Si
S
O
Ne
Mg
C
Ar
Ca
He
H
N

FIGURE 1a

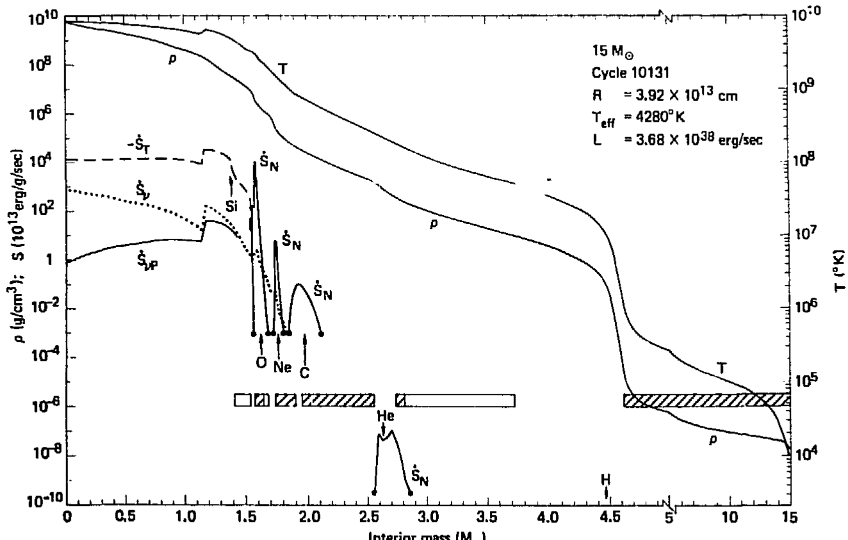
15 $M_\odot$
Cycle 10131
R = 3.92 X 10^{13} cm
T_{eff} = 4280°K
L = 3.68 X 10^{38} erg/sec
ρ
T
$-\dot{S}_T$
$\dot{S}_\nu$
$\dot{S}_{\nu P}$
$\dot{S}_N$
Si
O
Ne
C
He
H
ρ (g/cm^3); S (10^{13}erg/g/sec)
T (°K)
Interior mass ($M_\odot$)

FIGURE 1b

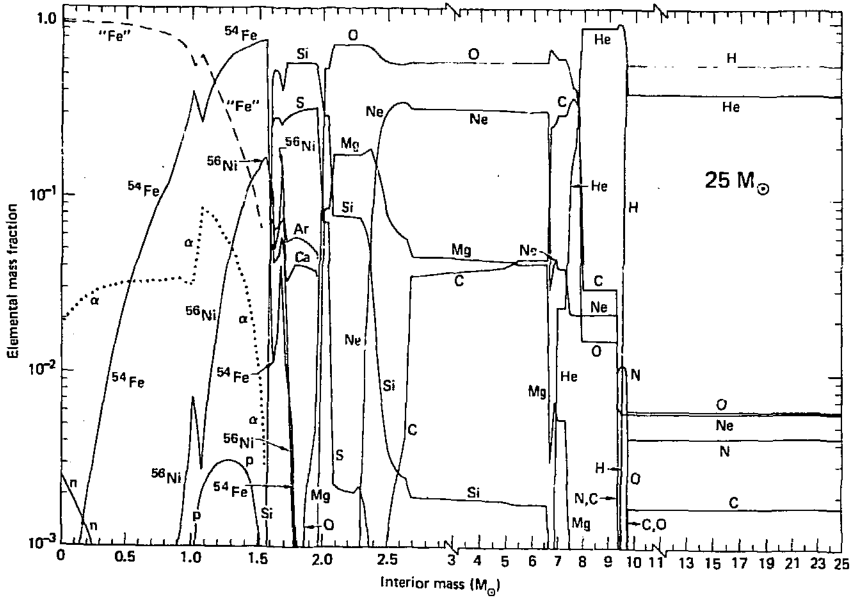
25 M⊙
Elemental mass fraction
Interior mass (M⊙)
"Fe"
54Fe
56Ni
α
Si
S
Ar
Ca
O
Ne
Mg
C
He
H
N
p
n
FIGURE 2a

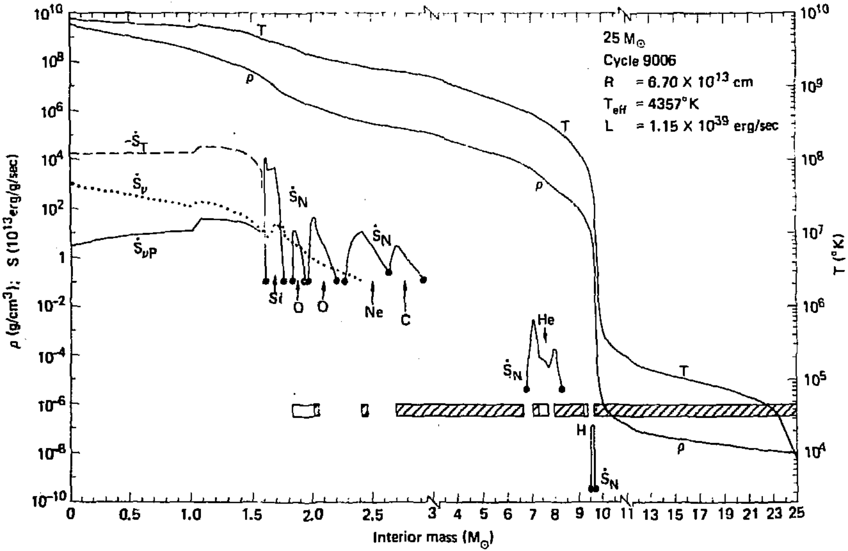
25 $M_\odot$
Cycle 9006
R = 6.70 X 10^{13} cm
T_{eff} = 4357°K
L = 1.15 X 10^{39} erg/sec
ρ (g/cm^3); S (10^{13}erg/g/sec)
T (°K)
Interior mass ($M_\odot$)
T
ρ
$-\dot{S}_T$
$\dot{S}_\nu$
$\dot{S}_{\nu P}$
$\dot{S}_N$
Si
O
O
Ne
C
He
H

FIGURE 2b

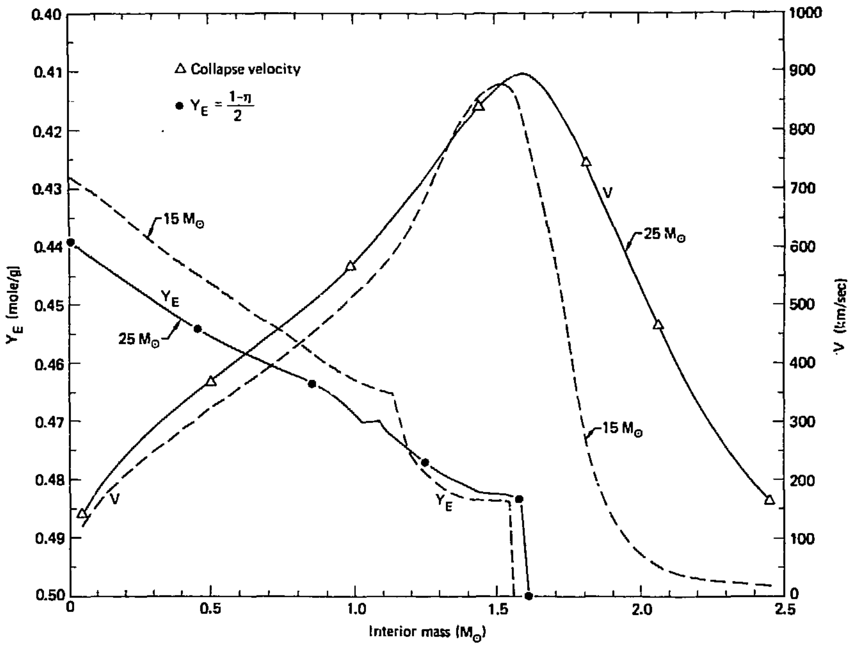

△ Collapse velocity
● $Y_E = \frac{1-\eta}{2}$
15 M☉
Y_E
25 M☉
V
25 M☉
15 M☉
Y_E
V
Y_E (mole/g)
V (km/sec)
Interior mass (M☉)
0.40
0.41
0.42
0.43
0.44
0.45
0.46
0.47
0.48
0.49
0.50
1000
900
800
700
600
500
400
300
200
100
0
0
0.5
1.0
1.5
2.0
2.5

FIGURE 3

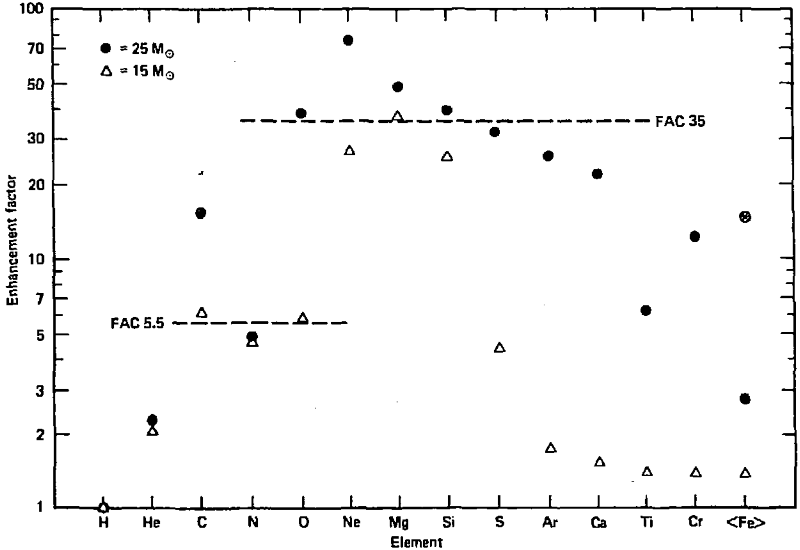

100
70
50
30
20
10
7
5
3
2
1
Enhancement factor
● = 25 M☉
Δ = 15 M☉
FAC 35
FAC 5.5
H
He
C
N
O
Ne
Mg
Si
S
Ar
Ca
Ti
Cr
<Fe>
Element

FIGURE 4